REFINEMENT OF A SEMI-EMPIRICAL METHOD FOR THE ESTIMATION OF PROFILE VORTEX SHEDDING FREQUENCY FROM LOW-SPEED AXIAL FAN BLADE SECTIONS

E. Balla - J. Vad

Department of Fluid Mechanics, Faculty of Mechanical Engineering, Budapest University of Technology and Economics, Bertalan Lajos u. 4-6., H-1111 Budapest, Hungary; Email: balla@ara.bme.hu, vad@ara.bme.hu

ABSTRACT

In the paper, a semi-empirical modeling method is presented for the estimation of the frequency of profile vortex shedding occurring in low-speed axial fans. The model uses parameters that are already available in the design process of fans, namely the drag coefficient, the zero-lift based angle of attack, the chord, and the relative thickness of the blade. The model has been defined based on measurement data on symmetrical and non-symmetrical blades between 2% to 25% relative thickness and up to 10° angle of attack. The precision of the model allows to determine the third octave band at which profile vortex shedding may occur.

KEYWORDS

vortex shedding, low Reynolds number, axial fan, aeroacoustics

NOMENCLATURE

b	distance between vortex rows [m]
c	chord [m]
C_D	drag coefficient [-]
d_{TE}	trailing edge thickness [m]
D	drag force acting on unit span [N/m]
f	frequency [Hz]
K	frequency scaling factor [-]
K^*	wake momentum thickness based frequency scaling factor [-]
Re	chord based Reynolds number [-]
St^*	universal Strouhal number [-]
t	maximum thickness [m]
U_0	free-stream velocity [m/s]
v	local velocity [m/s]
Y	spatial coordinate perpendicular to the chord and the span [m]
α	angle of attack [°]
δ	boundary layer thickness [m]
ϵ	uncertainty [-]
ν	kinematic viscosity [m^2/s]
ρ	density of fluid [kg/m^3]
σ	uncorrected standard deviation [%]
θ	wake momentum thickness [m]

Subscripts	
L	zero-lift based
lit	literature
mean	time averaged value
meas	measured
P	pressure side
RMS	root-mean-square
S	suction side
TE	trailing edge
Abbreviation	
PVS	profile vortex shedding
TE	trailing edge

INTRODUCTION

Low-Reynolds number fans are widely used in human environment (Huang, 2003, Borges, 2012, Gue et al., 2011), which makes their silent operation a priority. According to Dou et al. (2016) one of the prominent noise sources of low speed axial fans is the profile vortex shedding (PVS) noise. PVS is the periodic shedding of coherent vortices over the lifting surface of the blade. PVS is related to Tollmien-Schlichting instability waves originating in the laminar boundary layer upstream of the trailing edge (TE) (Daku and Vad, 2020). This noise class is referred to in Brooks et al. (1989) as laminar-boundary-layer-vortex-shedding noise. The reason for the latter terminology is that according to Brooks et al. (1989), a precondition for the occurrence of PVS is the existence of laminar boundary layer over most of at least one side of an airfoil. However, as reported in Yarusevych and Boutilier (2011), vortices may shed from the profile even if the initially laminar boundary layer, being separated in the vicinity of the leading edge, exhibits laminar-to-turbulent transition and reattachment upstream of mid-chord position. Therefore, the generalized term of PVS noise is used herein instead of using the term in Brooks et al. (1989). Longhouse (1977) conducted investigations on realistic fan rotors, focusing on the occurrence of PVS. He concluded that PVS noise can be significant and should be considered in the design of fans for minimum noise. As an illustration for such conclusion, he presented a sound pressure spectrum with a remarkable peak of PVS noise, although the occurrence of PVS was confined to some percent of the blade span near the tip of a single blade of the four-bladed rotor. He pointed out that the PVS phenomenon may be suppressed by means of boundary layer tripping. It is noted, however, that such modifications are to be treated with criticism for realistic fans, given that boundary layer tripping may moderate the aerodynamic performance of the fan (Lowson et al., 1994). In Longhouse (1977), it was stated that the frequency of PVS does not scale directly with the flow velocity thus further studies are needed for the establishment of a frequency scaling law. Based on the above, in order to be able to decrease the noise emission of fans, a model would be desirable, which is capable of forecasting the frequency at which PVS may occur, already in the design phase.

The aim of the paper is to establish a semi-empirical model for the estimation of the frequency of PVS noise. The present research contains data on moderate chord based Reynolds numbers, in the order of magnitude $10^4 - 10^6$. The chord based Reynolds number is defined as follows

$$Re = \frac{cU_0}{\nu} \tag{1}$$

where c is the chord length, U_0 is the free-stream velocity, and ν is the kinematic viscosity of the fluid. In the present paper, low-speed fans are defined as fans operating at $Re \leq 10^5$. The investigation involves blade sections being characteristic for low-speed axial fans.

The proposed semi-empirical model is a summary, reformulation, and extension of theories and measurement results already available in the literature. It is a summary since it gathers the theoretical

and measurement results of various authors. It is a reformulation since, instead of the current recommendations available in the literature, it uses a more straightforward, integral-based parameter for characterizing the viscous flow in the vicinity of the blade. It is also an extension as the method in current literature is based on measurements on a specific profile, the NACA0012, while the authors' investigation takes various profile geometries into account, including asymmetrical profiles.

The studies presented herein are related either to rectilinear blade / airfoil profiles modeling radially stacked blades or to unskewed rotor blades. This choice is in accordance with the fact that a significant portion of the "propeller-type" industrial axial fans available on the market are equipped with radially stacked blading, for which case studies are illustrated in Masi and Lazzaretto (2019).

THEORETICAL BACKGROUND

In Yarusevych et al. (2009) the notion of universal Strouhal number, St^* was introduced for profile vortex shedding and was defined based on the distance between the shed vortex rows.

$$St^* = \frac{fb}{U_0} \tag{2}$$

where f is the frequency of vortex shedding, b is the distance between the shed vortex rows, as illustrated in Figure 1, and U_0 is the free-stream velocity. In Yarusevych and Boutilier (2011) the value of $St^* = 0.16$ was proposed. As it will be discussed later on, based on Departmental measurements reported in Daku and Vad (2020), the authors find the approximation of $St^* = 0.16$ valid for the whole investigation range.

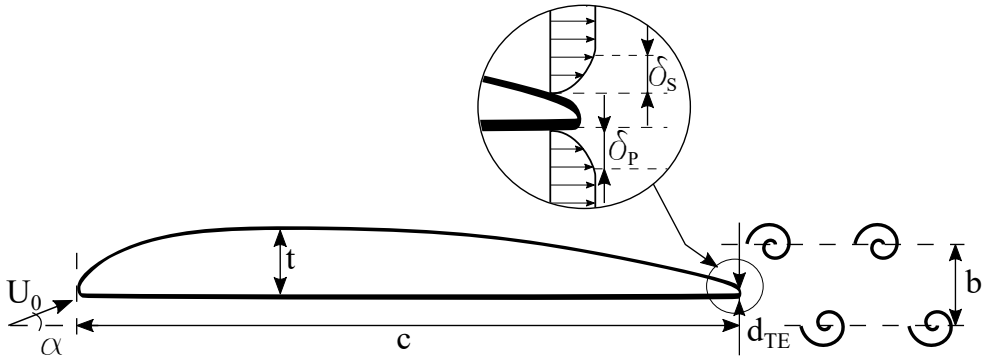

Figure 1: **Sketch of profile vortex shedding with the indication of characteristic quantities**

According to Equation (2), in order to be able to estimate the vortex shedding frequency, the b distance has to be determined first. The measurement of b is a cumbersome process since, depending on the size of the blade, distances ranging from tenths to a few millimeters have to be measured in a transient environment. However, the literature (Dou et al., 2016, Lee et al., 1993, Hersh et al., 1974, Fathy et al., 1977) proposes an empirical equation for the determination of b.

$$b = K\delta + d_{TE} \tag{3}$$

where K is a frequency scaling parameter, δ is the total boundary layer thickness, and d_{TE} is the TE thickness of the blade. The value of K has been determined in the literature based on experimental studies on NACA0012 airfoils to be $K \approx 0.5 - 0.6$, which corresponds to a 20% uncertainty. It is to be emphasized that the applicability of Equation (3) in realistic fan cases is doubtful since the δ total boundary layer thickness is uncertain to determine due to the complexity of rotor flow. Instead of δ introducing an integral-based parameter, such as the wake momentum thickness is therefore desirable. Thus Equation (3) has been reformulated by the authors as follows

$$b = K^*\theta \tag{4}$$

where K^* is the wake momentum thickness based frequency scaling parameter, and θ is the wake momentum thickness. According to Lee et al. (1993) and Fathy et al. (1977) the drag force acting on unit span is

$$D = \rho U_0^2 \theta \tag{5}$$

where ρ is the density of the fluid. Equation (5) can be deduced from the streamwise component of the momentum equation. The drag coefficient can be formed by nondimensionalizing Equation (5)

$$C_D = \frac{D}{\rho \frac{U_0^2}{2} c} = \frac{2\theta}{c} \tag{6}$$

where c is the chord of the blade. From Equation (6), θ/c can be expressed

$$\frac{\theta}{c} = \frac{C_D}{2} \tag{7}$$

This means that by knowing the drag coefficient of any profile, the momentum thickness per chord can be calculated. Through the drag coefficient, the proposed model is capable of taking various profile geometries into account. Ideally, C_D is available from measurements, however in absence of such results, reliable Computational Fluid Dynamic simulations (Morgado et al. 2016) can also be utilized as data source for the drag coefficient.

From Equations (2), (3) and (7) the vortex shedding frequency can be estimated in possession of the corresponding C_D, c, K^*, U_0 and St^*. The process of the frequency estimation is depicted in Figure 2. Re is the Reynolds number, and α_L is the zero-lift based angle of attack. The determination of K^*, along with the details of the new model and the definition of α_L, will be discussed later on.

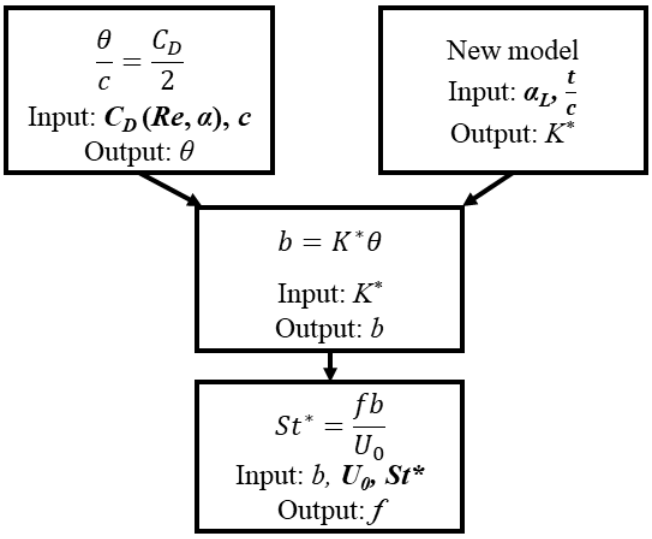

Figure 2: **Flowchart presenting the process of PVS frequency estimation. The independent input parameters are in bold**

SUPPLEMENTARY STUDY ON NON-SYMMETRICAL PROFILES

The PVS studies reported in the literature are related predominantly to symmetrical blade profiles. Hot-wire measurements were performed (Daku and Vad, 2020), in order to determine the frequency of PVS for non-symmetrical profiles as well. A circular-arc cambered plate with 8% camber and blunt edges and the RAF6-E profile (see Figure 1) were under investigation. The RAF6-E airfoil profile has been chosen as being representative in fan design in accordance with the classic fan design handbook

by Wallis (1961). It represents an intermediate geometry between symmetrical airfoil profiles (e.g. the NACA00 series) and cambered airfoil profiles used in realistic axial fans since it is a profile with flat pressure side and moderately curved camber line. The authors' previous research also included data regarding the lift and drag coefficients of the RAF6-E profile (Balla and Vad, 2019). The measurements were carried out at $Re = 0.6 \cdot 10^5 - 1.4 \cdot 10^5$ and at $\alpha = 0° - 10°$, for both the RAF6-E and the cambered plate.

The frequency of PVS was measured. Furthermore, according to Figure 2, the drag coefficients are also necessary for the determination of K^*. To the authors' best knowledge, no measurement data, corrected for three dimensional effects (e.g. the effect of tip clearance or the vicinity of the wall) is available at such low Reynolds numbers for the C_D of the RAF6-E airfoil. Neither does a model exist for the calculation of C_D in case of the RAF6-E airfoil. However, the drag coefficient can be calculated from θ according to Equations (6) and (7). During the hot-wire measurements, the velocity distribution in the wake of the profiles was monitored. A representative example is shown in Figure 3. v_{mean} is the local time-averaged velocity, v_{RMS} is the local root-mean-square of the velocity, Y is the spatial coordinate perpendicular to the chord and the span. The velocity at the wake boundaries was taken as the arithmetic mean value of the velocities measured at the outermost positions of the hot-wire wake traverse for all cases with the same Re and same profile geometry. The wake velocity profile was normalized by the aforementioned mean value. The wake momentum thickness θ was computed using this normalized wake velocity profile with numerical integration by means of the trapezoidal rule built-in function of the MATLAB R2019b software (Schlichting and Gersten, 2016, Atkinson, 1989). From θ, C_D was determined for the RAF6-E airfoil, with Equations (6) and (7), and is presented in Figure 4. The obtained measurement-based C_D value of the RAF6-E airfoil could only be compared qualitatively with literature data (Wallis, 1961) since no measurement data (corrected for three dimensional effects) or quantitative model exist in the literature for the C_D of the RAF6-E airfoil at these Re. The comparison is shown in Figure 4, the data points at Re = 300 000 were taken from the literature. The value of C_D is increasing with the decrease of Re, as expected, based on Balla and Vad (2019).

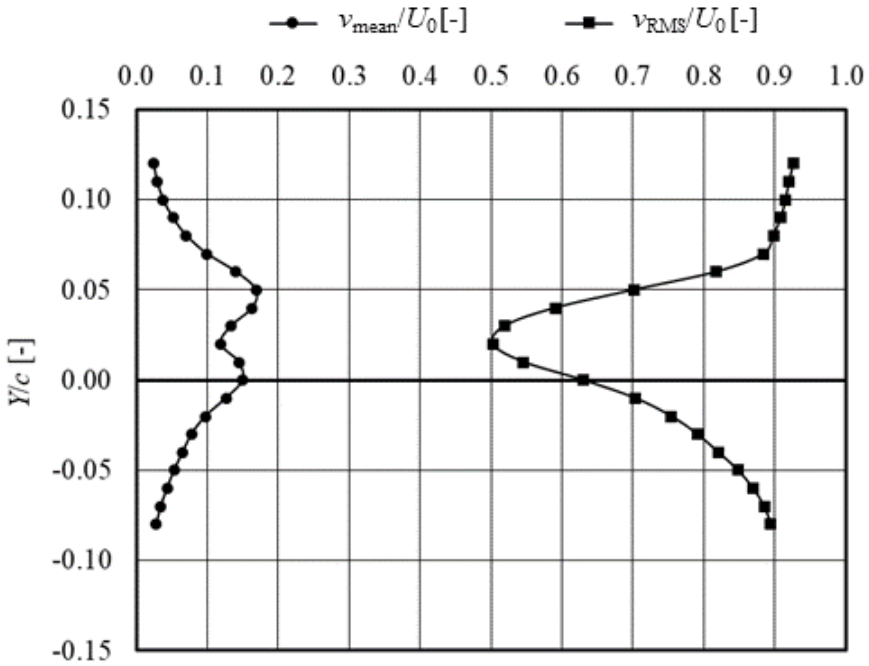

Figure 3: **Velocity in the wake of the RAF6-E profile at** $\alpha = 0°$ **and** $Re = 60000$

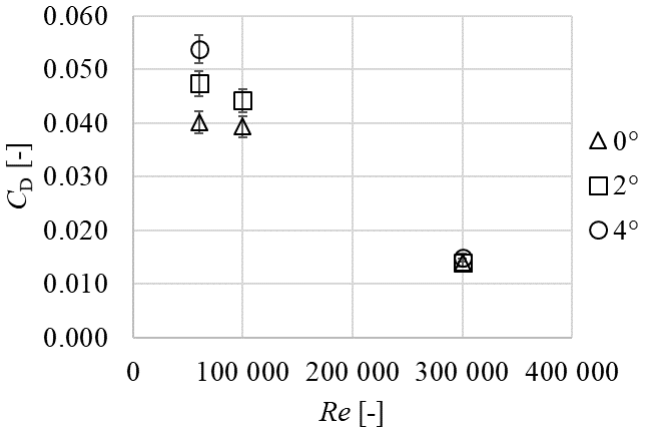

Figure 4: **Measurement-based drag coefficients for the RAF6-E airfoil**

With the above calculations of C_D, the measurements reported in Daku and Vad (2020) could be treated together with data taken from other literature sources for further processing. For further calculations, the measurement-based C_D is used for the RAF6-E airfoil, and the model-based C_D is used for the cambered plate. The model-based value was determined by calculating C_D for a case with rounded leading and TE, with an empirical model based on Balla and Vad (2020), and then adding the effect of edge bluntness, based on measurements reported in Balla (2020).

DETERMINATION OF MODEL PARAMETERS

The case studies used for the determination of K^* are summarized in Table 1. The cases were obtained from references: Yarusevych et al. (2009), Yarusevych and Boutilier (2011), Paterson et al. (1973), Brooks et al. (1989), Hersh et al. (1974), De Gennaro and Kuehnelt (2012), Daku and Vad (2020). A more detailed description of each case is included in Balla and Vad (2019b). In Table 1, the first column indicates the serial number of the case under discussion. In the second, "Profile" column, the types of the profiles are specified. The cross-section of the cambered plate is shown in Figure 5. t/c is the maximum relative thickness, defined as presented in Figure 5. In the next column, the angle of attack based on zero lift α_L is the angle between a theoretical free stream direction, at which the profile produces zero lift and the actual flow direction U_0. Such angle of attack definition was also used by De Gennaro and Kuehnelt (2012). At $\alpha_L = 0°$, the profiles produce zero lift. On the other hand, α is the geometrical angle, measured between the chord c and the free-stream velocity U_0. For symmetrical profiles $\alpha_L = \alpha$. Based on the literature, $\alpha_L = 0°$ corresponds approximately to $\alpha = -8°, -5°$, and $-4°$ for the NACA4509 (De Gennaro and Kuehnelt, 2012), the RAF6-E and the cambered plate with $h/c = 8\%$ (Wallis, 1961), respectively. Figure 5 indicates $\alpha_L = 0°$ and $\alpha = 0°$ for the cambered plate under investigation. The column "St^*" in Table 1 contains the values of the universal Strouhal number for each case. "St^*" could only be calculated for a minority of cases with Equation (2). These cases included measurements regarding b: Yarusevych et al. (2009), Yarusevych and Boutilier (2011), and Daku and Vad (2020). For those cases where it was not possible to determine St^* from the measurement data, the value of $St^* = 0.16$ was used in accordance with Yarusevych and Boutilier (2011). For each case, the K^*_{meas} parameter was determined from f as a result of a reverse process based on Figure 2. An estimation was made for the uncertainties of K^*_{meas}. ϵ_{meas} was calculated based on the data available on the measurement setups reported in the literature. The details of the uncertainty calculations are summarized in Balla and Vad (2019b). $K^*_{modeled}$ was determined with the use of the K^*, deduced in the forthcoming paragraphs. $\epsilon_{modeled}$ is the relative discrepancy of $K^*_{modeled}$ compared to K^*_{meas}. The investigated Reynolds number range was between Re= 55 000 and Re=1.5 million. The range is in accordance with the limiting Reynolds number

corresponding to the PVS phenomenon and described in detail in Balla and Vad (2019b). The K^*_{meas} values, presented in Table 1 were determined independently from the Reynolds number. According to the authors' investigation, the Reynolds number variance only had a negligible effect on the value of K^*_{meas}.

Table 1: **Investigated geometries and calculated parameters**

#	Profile	t/c [%]	$\alpha_L[^\circ]$	St^*	K^*_{meas}	ϵ_{meas}	$K^*_{modeled}$	$\epsilon_{modeled}$
1	NACA0025	25	0	0.185	7.1	4%	6.6	-7%
2			5	0.160	5.7		6.0	5%
3			10	0.145	4.4		4.3	-2%
4	NACA0018	18	10	0.155	3.1	3%	3.0	-3%
5				0.160	2.2	13%	3.0	36%
6	NACA0012	12	0		5.0	13%	4.1	-18%
7			3		4.1		4.0	-2%
8			4		3.6		3.8	6%
9			5		3.2		3.6	13%
10			4		4.1	14%	3.8	-7%
11			0		6.6	13%	4.1	-38%
12			4		4.7	13%	3.8	-19%
13			6		3.0		3.4	13%
14			10		2.6		1.9	-27%
15	NACA4509	9	9		2.9	12%	2.1	-28%
16	RAF6-E	10	5	0.180	1.9	12%	3.2	68%
17			7	0.170	1.7		2.7	59%
18			9	0.100	1.8		1.9	6%
19	Cambered plate	2	6	0.170	1.3		1.5	15%
20			8	0.180	1.1		0.8	-27%

Figure 5: **Cambered plate with relative camber $\mathrm{h/c} = 8\%$, with indication of the maximum blade thickness t and the chord length c. The angle of attack α, and the zero lift based angle of attack α_L is represented with three examples**

The measurement points are plotted in Figure 6 in the function of α_L. K^*_{meas} tends to decrease as α increases for symmetrical profiles. The change in t/c only causes a shift in the K^*_{meas} values, the shape of the fitted curves remains the same. From the K^*_{meas} values, a general model for K^* is established in the following. Data points were grouped according to the corresponding t/c values. Second order polynomials were fitted to each group. For all symmetrical profiles, for which most data points were available, the best fit could be achieved when the coefficient of the second order term was approximately -0.023. The dependence on t/c can be taken into account with the shift of $K^*(\alpha_L = 0^\circ)$. The relation between $K^*(\alpha_L = 0^\circ)$ and t/c was assumed to be linear. Thus, the value of K^* can be calculated with the use of the following expression

$$K^* = 1.9 + 0.19\frac{t}{c} - 0.023\alpha_L^2 \tag{8}$$

where t/c is in percent and α_L is in degrees. The empirical correlation in Equation (8) takes a nonzero value (i.e. 1.9) even for zero t/c and α_L values. The above suggests that even the boundary layers developing over the two surfaces of an infinitely thin flat plate at $\alpha = 0°$, and interacting past the TE may cause vortex shedding. This assumption is supported by the findings of Chase (1972) and Voke and Potamitis (1994).

The curves calculated with Equation (8), along with the measurement points, are presented in Figure 6. The size of the error bars has been determined as the highest ϵ_{meas} uncertainties corresponding to each t/c in Table 1.

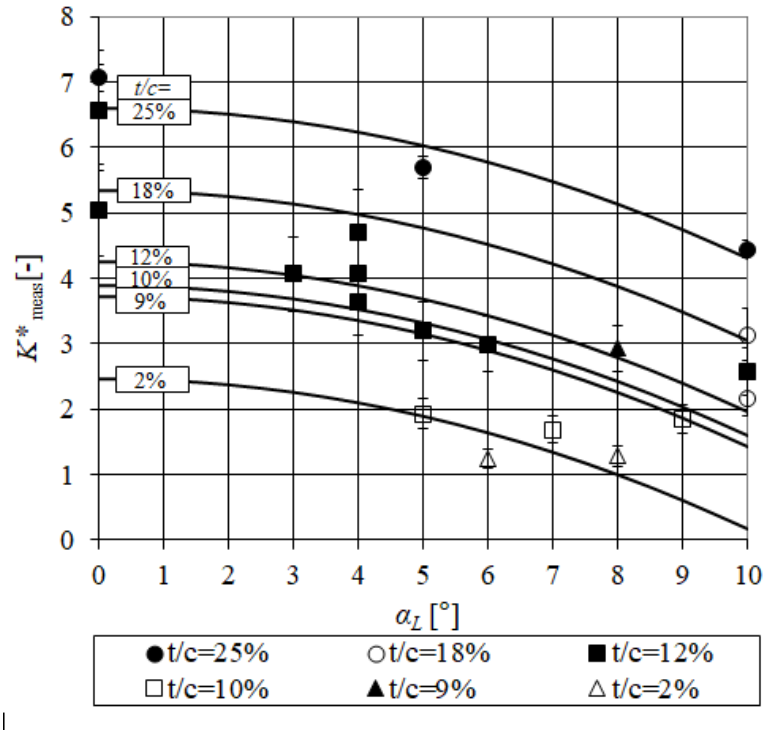

Figure 6: **The value of K^*_{meas} as a function of angle of attack for different maximum relative blade thicknesses. Solid lines indicate the modeled curve for each maximum relative blade thickness, and the markers indicate the measurement points**

UNCERTAINTY ANALYSIS

In order to estimate the overall uncertainty of the empirical model formulated in Equation (8), the value of K^* for each case was determined using Equation (8) ($K^*_{modeled}$) and was compared to the values calculated from measurement data (K^*_{meas}). The values of $K^*_{modeled}$ along with the relative discrepancy, $\epsilon_{modeled}$ are shown in Table 1. A statistical sample was generated from $\epsilon_{modeled}$. The uncorrected standard deviation of such a sample is considered as a single-value metric quantifying the error of the semi-empirical model presented herein. The uncorrected standard deviation of the aforementioned sample has been calculated to be $\sigma_{\epsilon,modeled} = \pm 27\%$. A comparison of measurement-based and modeled K^* is presented in Figure 7. The thick black line represents perfect match between the measurements and the model. The region between the gray lines indicates the model uncertainty $\sigma_{\epsilon,modeled}$. It can be concluded that taking into consideration the model uncertainty, the model estimates almost all points within their measurement uncertainty. The highest obtained $\epsilon_{modeled}$ occurs for the RAF6-E profile. A possible explanation is that compared to symmetric profiles, in case of non-symmetric profiles K^* shows only moderate angle of attack dependence. A thorough future research on non-symmetric profiles offers more insight into this behavior.

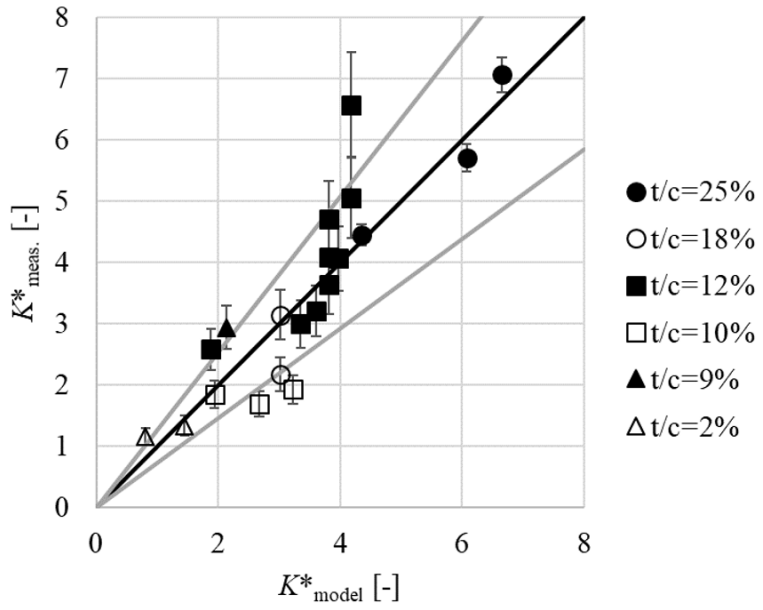

Figure 7: **Comparison of the measured and modeled K*. The thick black line represents perfect match between the measurements and the model. The region between the gray lines indicates the model uncertainty** $\sigma_{\epsilon,\mathbf{modeled}}$

In order to be able to compare the new model to the already existing one in the literature, characterized by Equation (3), equivalent K^*_{lit} were calculated based on $K \approx 0.5 - 0.6$. Combining Equations (3) and (4) yields:

$$K^*_{lit} = \frac{K\delta + d_{TE}}{\theta} \tag{9}$$

Calculations were made with K set to 0.5 (Fathy et al., 1977) and 0.6 (Dou et al., 2016, Lee et al., 1993, Hersh et al., 1974). δ was unknown for most cases, and to the authors' best knowledge, no generalized relationship exists in the literature for δ. In absence of generalized empirical modelling of δ, the authors refer to the empirical model established by Brooks et al. (1989) (BPM model), in which uniquely detailed data are provided for estimating θ, δ, and their ratio δ/θ on the basis of measurements on NACA0012 airfoils. Even though it was originally developed for the symmetrical NACA0012 profile, the BPM model has already been applied successfully to the noise prediction of non-symmetric profiles (De Gennaro and Kuehnelt, 2012, Migliore and Oerlemans, 2004). According to the BPM model, θ and δ can be calculated as

$$\theta = \theta_S + \theta_P \tag{10}$$

$$\delta = \delta_S + \delta_P \tag{11}$$

where the subscripts S and P denote values corresponding to the suction and pressure side, respectively. The δ/θ ratio can be calculated using the empirical formulae of the BPM model. Only the Reynolds number and the angle of attack are the necessary input parameters for calculating δ/θ. K^*_{lit} can now be calculated with Equation (9) using the ratio δ/θ and θ from Equation (7). K^*_{lit} is presented in Table 2 for both K=0.5 and K=0.6 in the same column, separated by a comma. For comparison $K^*_{modeled}$, calculated with the new model developed by the authors, is also presented in Table 2. ϵ_{lit} is the relative discrepancy of K^*_{lit} compared to K^*_{meas}, presented in Table 1.

Table 2: **Comparison of the discrepancies of the new model and the one already existing in the literature. The K^*_{lit} and ϵ_{lit} columns contain the values corresponding to the K=0.5 and the K=0.6 value, separated by a comma.**

#	$K^*_{modeled}$	$\epsilon_{modeled}$	K^*_{lit}	ϵ_{lit}
1	6.6	-7%	4.8, 5.7	-32, -19%
2	6.0	5%	4.0, 4.7	-30, -17%
3	4.3	-2%	3.5, 4.2	-21, -6%
4	3.0	-3%	3.5, 4.1	10, 32%
5	3.0	36%	3.5, 4.2	60, 93%
6	4.1	-18%	4.8, 5.7	-6, 12%
7	4.0	-2%	4.4, 5.3	9, 30%
8	3.8	6%	4.3, 5.0	17, 39%
9	3.6	13%	4.0, 4.8	26, 50%
10	3.8	-7%	4.1, 4.9	1, 20%
11	4.1	-38%	4.7, 5.6	-29, -15%
12	3.8	-19%	4.2, 5.0	-10, 7%
13	3.4	13%	3.8, 4.5	26, 49%
14	1.9	-27%	3.5, 4.2	37, 63%
15	2.1	-28%	5.3, 6.4	81, 117%
16	3.2	68%	2.0, 2.4	6, 24%
17	2.7	59%	1.8, 2.2	8, 28%
18	1.9	6%	1.9, 2.3	6, 24%
19	1.5	15%	2.3, 2.6	71, 98%
20	0.8	-27%	1.6, 1.8	35, 55%

$\sigma_{\epsilon,lit}$ was calculated in the same manner as $\sigma_{\epsilon,modeled}$ and was found to be 31% and 37% for K=0.5 and K=0.6, respectively. Thus, the newly developed model established herein outperforms the previous model based on Equation (3) in the literature. Besides, it offers a more straightforward and reliable estimation by using only geometrical parameters and the mostly accessible C_D.

For the estimation of the PVS frequency, f, both St^* and K^* are necessary, and their uncertainties are independent from each other. The average value and the uncorrected standard deviation were calculated for St^*, their values being $\overline{St^*} = 0.16$ and $\sigma_{St^*} = 12\%$, respectively. This confirms the universality of the St^* Strouhal number (Yarusevycvh et al., 2009), even with the extension to blade profiles used in low-speed axial fan design (Daku and Vad, 2020). From the above, the overall uncertainty for the estimation of f was calculated to be $\sigma_f = 30\%$. In engineering practice, this level of uncertainty still offers the possibility to identify the third-octave frequency band corresponding to the PVS noise. According to the recent study of Yakhina et al. (2020), the PVS noise may consist of several tones spreading in a frequency range of a few hundred Hz. In order to decrease the harmful impact of noise on humans caused by PVS, the occurrence of PVS may be accepted, but its broadband frequency hump being characteristic for a realistic fan, should be moved away from the third-octave bands characterized by the highest A-weights (Benedek and Vad, 2016, Norton and Karczub, 2003) by means of appropriate blade design. The frequency hump of PVS noise may be as broad as +/- 40 % of the central frequency (Yarusevych and Boutilier, 2011). Therefore, the ambition to estimate the PVS frequency with a third-octave-band resolution using the present semi-empirical model is judged reasonable. If the mistuning of PVS farther away from the plateau of the A-weighting graph cannot be realized by blade design means, an alternate way is to carry out modifications on the blade layout for suppression of the PVS phenomenon in itself, e.g. by means of boundary layer tripping (Longhouse, 1977).

CONCLUSION AND FUTURE REMARKS

A semi-empirical model was established for the prediction of the frequency of PVS for various blade geometries. Using the model, the third octave frequency band, which may be affected by PVS can be determined. With appropriate fan redesign, vortex shedding at the bands with the highest A-weight may be avoided. For the estimation of the frequency, only geometrical and operational data as well as the drag coefficient are required. Compared to previous methods in the literature, the model takes into account the effect of maximum relative blade thickness and the angle of attack and is applicable for both symmetric and non-symmetric profiles.

In the future, the investigations on isolated blade models are to be extended to stationary and rotating blade cascades in order to examine the applicability of the semi-empirical model to realistic rotors. Taking the effect of camber, and the asymmetry of the camber line into account in the semi-empirical model also offers a possibility for improvement.

ACKNOWLEDGEMENTS

The research reported in this paper and carried out at BME has been supported by the NRDI Fund (TKP2020 IES, Grant No. BME-IE-WAT) and by the NRDI Fund (TKP2020 NC, Grant No. BME-NCS) based on the charter of bolster issued by the NRDI Office under the auspices of the Ministry for Innovation and Technology. The research has also been funded by the Hungarian National Research, Development and Innovation Centre under contract No. K 129023, and the National Talent Programme of the Ministry of Human Capacites, Hungary (NFTO-20-B-0232).

REFERENCES

Atkinson, K., An introduction to numerical analysis, 2nd ed., Hoboken: John Wiley & Sons, 1989.

Balla, E., "Aerodynamic and aeroacoustic behavior of axial fan blade sections at low Reynolds numbers," PhD dissertation, 2020.

Balla, E., Vad, J., "Lift and drag force measurements on basic models of low-speed axial fan blade sections," Proceedings of the Institution of Mechanical Engineers, Part A: Journal of Power and Energy, vol. 233, no. 2, pp. 165-175, 2019.

Balla, E., Vad, J., "A semi-empirical modell for predicting the frequency of profile vortex shedding relevant to low-speed axial fan blade sections," in The 13th European Conference on Turbomachinery Fluid Dynamics and Thermodynamics, Lausanne, Switzerland, Paper ID: 311, 12p., 8-12 April 2019.

Balla, E., Vad, J., "An empirical model to determine lift and drag coefficients of cambered plates at moderate Reynolds numbers," Proceedings of the Institution of Mechanical Engineers, Part A: Journal of Power and Energy, Online first, 2020.

Benedek, T., Vad, J., "An industrial on-site methodology for combined acoustic-aerodynamic diagnostics of axial fans, involving the phased array microphone technique," International Journal of Aeroacoustics, vol. 15, no. 1-2, pp. 81-102, 2016.

Borges, S.S., "CFD techniques applied to axial fans design of electric motors," in Proc. International Conference on Fan Noise, Technology and Numerical Methods (FAN2012), Senlis, France, 18-20 April 2012.

Brooks, T.F., Pope, D.S., Marcolini, M.A., "Airfoil Self-Noise and Prediction," NASA Ref. Publication 1218, 1989.

Chase, D.M., "Sound radiated by turbulent flow off a rigid half-plane as obtained from a wavevector spectrum of hydrodynamic pressure," The Journal of the Acoustical Society of America, vol. 52, no. 3B, pp. 1011-1023, 1972.

Daku G., Vad J., "Experiment-based preliminary design guidelines for consideration of profile vortex shedding from low-speed axial fan blades," in Proc. ASME Turbo Expo 2020, London, UK, Paper ID: GT2020-14214, June 22-26, 2020.

De Gennaro, M., Kuehnelt, H., "Broadband noise modelling and prediction for axial fans," in Pro-

ceedings of the Internataional Conference Fan Noise, Technology and Numerical Methods, Senlis, France, p. 12., 18-20 April 2012.
Dou, H., Li, Z., Lin, P., Wei, Y., Chen, Y., Cao, W., He, H., ”An improved prediction model of vortex shedding noise from blades of fans,” Journal of Thermal Science, vol. 25, no. 6, pp. 526-531, 2016.
Fathy, A., Rashed, M.I., Lumsdaine, E.,”A theoretical investigation of laminar wakes behind airfoils and the resulting noise pattern,” Journal of Sound and Vibration, vol. 50, no. 1, pp. 133-144, 1977.
Gue, F., Cheong, C., Kim, T., ”Development of low-noise axial cooling fans in a household refrigerator,” Journal of Mechanical Science and Technology, vol. 25, pp. 2995-3004, 2011.
Hersh, A.S., Sodermant, P.T., Hayden, R.E., ”Investigation of acoustic effects of leading-edge serrations on airfoils,” Journal of Aircraft, vol. 11, no. 4, pp. 197-202, 1974.
Huang, L.X., ”Characterizing computer cooling fan noise,” The Journal of the Acoustical Society of America, vol. 114, pp. 3189-3200, 2003.
Lee, C., Chung, M.K., Kim, Y.H., ”A prediction model for the vortex shedding noise from the wake of an airfoil or axial flow fan blades,” Journal of Sound and Vibration, vol. 164, no. 2, pp. 327-336, 1993.
Longhouse, R. E., ”Vortex shedding noise of low tip speed, axial flow fans,” Journal of Sound and Vibration, vol. 53(1), pp. 25-46, 1977
Lowson M., Fiddes S., Nash E., ”Laminar Boundary Layer Aeroacoustic Instabilities”, In: Proceedings of the 32nd Aerospace Sciences Meeting and Exhibit, Reno, NV, USA, 10-13 January, 1994.
Masi, M., Lazzaretto, A., ”A new practical approach to the design of industrial axial fans: tube-axial fans with very low hub-to-tip ratio”, ASME. Journal of Engineering for Gas Turbines and Power, 141(10): 101003, 2019.
Migliore, P., Oerlemans, S., ”Wind tunnel aeroacoustic tests of six airfoils for use on small wind turbines,” Journal of Solar Energy Engineering, vol. 126, no. 4, pp. 974-985, 2004.
Morgado, J., Vizinho, R., Silvestre, M., PÃ¡scoa, J., ”XFOIL vs CFD performance predictions for high lift low Reynolds number airfoils,” Aerospace Science and Technology, vol. 52, pp. 207-214, 2016.
Norton M., Karczub, D., Fundamentals of noise and vibration analysis for engineers, Cambridge: Cambridge University Press, 2003.
Paterson, R.W., Vogt, P.G., Fink, M.R., Munch, C.L., ”Vortex noise of isolated airfoils,” Journal of Aircraft, vol. 10, no. 5, pp. 296-302, 1973.
Schlichting H., Gersten, K., Boundary-layer theory, Berlin: Springer, 2016.
Voke, P.R., Potamitis, S.G., ”Numerical simulation of a low-Reynolds-number turbulent wake behind a flat plate,” International Journal for Numerical Methods in Fluids, vol. 19, no. 5, pp. 377-393, 1994.
Wallis, R.A., Axial flow fans, London: George Newnes Ltd., 1961
Yakhina G., Roger, M., Moreau, S., Nguyen, L., Golubev, V., ”Experimental and Analytical Investigation of the Tonal Trailing-Edge Noise Radiated by Low Reynolds Number Aerofoils,” Acoustics, vol. 2., no. 2., pp. 293-329, 2020.
Yarusevych S., Boutilier, M.S.H., ”Vortex Shedding of an Airfoil at Low Reynolds Numbers,” AIAA Journal, vol. 49, no. 10, pp. 2221-2227, 2011.
Yarusevych, S., Sullivan P.E., Kawall, J.G., ”On vortex shedding from an airfoil in low-Reynolds-number flows,” Journal of Fluid Mechanics, vol. 632, pp. 245-271, 2009.